Universidad Tecnológica Nacional
SEPTIEMBRE - DICIEMBRE 2026 / Año 24 - Nº 57

Revista Tecnología y Ciencia
DOI: https://doi.org/10.33414/rtyc.57.49-70.2026 - ISSN 1666-6933
licencia de Creative Commons - Reconocimiento-NoComercial 4.0 Internacional

Synthesis and Characterization of Waterborne Polyurethane-based Solid Polymer Electrolytes for Lithium-Ion Batteries

Síntesis y caracterización de electrolitos poliméricos sólidos basados en poliuretano de base acuosa para baterías de ion-litio

Presentado: 13/04/2026

Aprobado: 06/10/2026

Publicado: 06/11/2026

Agustín Vergalito
https://orcid.org/0009-0007-4313-880X
Universidad Tecnológica Nacional, Facultad Regional La Plata, Centro de Investigación y Desarrollo en Ciencias y Tecnología de Materiales UTN FRLP – CIC PBA, La Plata, Argentina.
avergalito@frlp.utn.edu.ar

Mariela Gisela Ortiz
https://orcid.org/0000-0003-4269-0321
Universidad Tecnológica Nacional, Facultad Regional La Plata, Centro de Investigación y Desarrollo en Ciencias y Tecnología de Materiales UTN FRLP – CIC PBA, La Plata, Argentina.
Instituto de Investigaciones Fisicoquímicas Teóricas y Aplicadas (INIFTA), Universidad Nacional de La Plata (UNLP), La Plata, Argentina.
mortiz@frlp.utn.edu.ar

Francisco Martín Pardini
https://orcid.org/0000-0002-3797-2917
Universidad Tecnológica Nacional, Facultad Regional La Plata, Centro de Investigación y Desarrollo en Ciencias y Tecnología de Materiales UTN FRLP – CIC PBA, La Plata, Argentina.
fpardini@frlp.utn.edu.ar

Abstract

Waterborne polyurethane (WPU) is a versatile matrix for developing solid polymer electrolytes (SPEs) for lithium-ion batteries. Its architecture contains ether groups within the

Revista Tecnología y Ciencia
DOI: https://doi.org/10.33414/rtyc.57.49-70.2026 - ISSN 1666-6933

polymer backbone, which promote coordination with lithium ions, thereby enhancing ionic mobility and improving the ionic conductivity of the material.

In this work, a WPU was synthesized and SPEs were subsequently prepared by incorporating lithium chloride (LiCl) at different concentrations into the polymer matrix. The obtained materials were characterized by Fourier transform infrared spectroscopy, X-ray diffraction, scanning electron microscopy, thermogravimetric analysis, differential scanning calorimetry, and electrochemical impedance spectroscopy.

The SPE sample containing 10 wt% LiCl exhibited the best performance, achieving an ionic conductivity of 2.82×10^{-7} S cm^{-1} at 25 °C, which is considered an adequate value for LiCl-based SPE systems.

Keywords: lithium-ion batteries; solid polymer electrolytes, waterborne polyurethane, ionic conductivity.

Resumen

El poliuretano en dispersión acuosa (WPU) es una matriz versátil para el desarrollo de electrolitos poliméricos sólidos (SPEs) en baterías de ion-litio. Su arquitectura presenta grupos éter en la cadena polimérica que favorecen la coordinación con iones de litio, lo que facilita la movilidad iónica y conductividad iónica del material.

En este trabajo se sintetizó un WPU y posteriormente se prepararon SPEs incorporando cloruro de litio (LiCl) en distintas concentraciones dentro de la matriz polimérica. Los materiales obtenidos fueron caracterizados mediante espectroscopía infrarroja por transformada de Fourier, difracción de rayos X, microscopía electrónica de barrido, análisis termogravimétrico, calorimetría diferencial de barrido y espectroscopía de impedancia electroquímica.

La muestra de SPE con 10 % en peso de LiCl mostró el mejor desempeño, alcanzando una conductividad iónica de $2{,}82 \times 10^{-7}$ S cm^{-1} a 25 °C, valor adecuado para sistemas de SPE basados en LiCl.

Palabras claves: baterías de ion-litio, electrolitos poliméricos sólidos, poliuretano en dispersión acuosa, conductividad iónica.

1. Introduction

Lithium-ion batteries (LIBs) currently represent one of the most relevant technologies for energy storage, owing to their high energy density and long cycle life during charge–discharge processes. These characteristics have enabled their widespread adoption in portable electronic devices, electric vehicles (EVs), and large-scale energy storage systems (Li et al., 2021; Lv et al., 2022; Tang et al., 2021).

The importance of this technology was formally recognized in 2019, when the Nobel Prize in Chemistry was awarded to John B. Goodenough, Michael S. Whittingham, and Akira Yoshino for their pioneering contributions to the development of LIBs. The advances derived from these pioneering studies have significantly driven the evolution of modern electronic devices and have contributed to improving the quality of life on a global scale (Andersson et al., 2022; Tang et al., 2021; Yang et al., 2020).

In LIBs, the electrochemical system consists of a cathode, an anode, a separator, and a liquid electrolyte. During battery operation, lithium ions (Li^+) are transported through the

Revista Tecnología y Ciencia
DOI: https://doi.org/10.33414/rtyc.57.49-70.2026 - ISSN 1666-6933

electrolyte between both electrodes throughout the charge and discharge processes (Li et al., 2021; D. Zhang et al., 2021; Zhu et al., 2014). However, the use of liquid electrolytes presents certain drawbacks associated with system safety, as they may exhibit leakage and pose risks of combustion or explosion, thereby compromising the overall safety of these batteries (Tu et al., 2021; Wu et al., 2019; Yang et al., 2020).

Simultaneously, the sustained growth of the portable electronic device and electric vehicle markets has created the need to develop batteries with higher energy storage capacity, improved performance at high charge–discharge rates, and greater power density, thereby driving the research and development of new materials and electrolyte configurations (Li et al., 2021; Yang et al., 2020).

In this context, solid polymer electrolytes (SPEs) have emerged as promising alternatives. These materials not only enhance safety by exhibiting lower flammability compared with liquid electrolytes, but also provide additional advantages, such as the mitigation of issues including self-discharge and intercell leakage, ease of processing for the fabrication of thin films, low cost, design flexibility, good interfacial contact with electrodes, and suitable ionic conductivity (Irfan et al., 2021; Larrabide et al., 2022; J. Wang et al., 2021).

In addition to PU-based systems, a variety of other polymer matrices have been explored as SPEs for LIBs. Poly(ethylene oxide) (PEO) remains the most widely studied host owing to its strong lithium-coordinating ability, although its practical use is limited by extensive crystallization at room temperature (Fenton et al., 1973; Misenan et al., 2022). Alternative matrices such as poly(acrylonitrile) (PAN), poly(methyl methacrylate) (PMMA), and poly(-vinylidene fluoride) (PVDF) have also been investigated, each offering a different balance of ionic conductivity, mechanical strength, and electrochemical and thermal stability (Ram Prasanth et al., 2025). In parallel, composite and hybrid electrolytes combining polymer matrices with ceramic or inorganic fillers, such as garnet-type (LLZO), NASICON-type, or perovskite-type oxide particles, have been developed to further enhance ionic conductivity and interfacial stability, at the expense of increased processing complexity (Yao et al., 2019).

Within the wide range of polymer electrolytes, polyurethanes (PUs) stand out as materials of considerable interest due to their characteristic segmented structure. These polymers are composed of soft segments, typically based on polyethers or polyesters, and hard segments derived from diisocyanates (Cui et al., 2024; Misenan et al., 2022). Polyether-based soft segments are capable of coordinating alkali metal salts, such as lithium salts, and exhibit high segmental chain mobility. This behavior facilitates ionic transport and contributes to the development of materials with enhanced ionic conductivity (Cui et al., 2024; Misenan et al., 2022). The hard segments function as physical cross-linking sites between the soft and hard domains, providing good mechanical properties. Consequently, the development of polymer electrolytes requires the concurrent optimization of ionic conductivity and mechanical integrity to enable the fabrication of thin films (Mustapa et al., 2021; Q. Zhang et al., 2021).

The synthesis of PU-based electrolytes is typically conducted through the reaction between linear poly(ethylene oxide) (PEO) and diisocyanates, leading to the formation of thermoplastic PUs with a linear structure. However, although PEO exhibits a high capacity to coordinate lithium salts at temperatures above 60–70 °C, this polymer tends to crystallize at room temperature (20–25 °C). This phenomenon significantly limits the ionic conductivity of the system (Cui et al., 2024; Fenton et al., 1973; Misenan et al., 2022).

Several strategies have been proposed in the literature to overcome this limitation, each involving specific advantages and drawbacks. The incorporation of low-molecular-weight plasticizers or ionic liquids increases segmental mobility and ionic conductivity (Özenler et al., 2025). However, this is often accompanied by a loss of mechanical integrity and, in the

Revista Tecnología y Ciencia
DOI: https://doi.org/10.33414/rtyc.57.49-70.2026 - ISSN 1666-6933

case of liquid plasticizers, leads to a partial compromise of the all-solid-state character of the electrolyte.

Similarly, the addition of ceramic or inorganic fillers can simultaneously disrupt polymer chain packing and reinforce the mechanical properties of the film (Yao et al., 2019). Nevertheless, achieving homogeneous filler dispersion and adequate polymer-to-filler interfacial contact remains challenging. Chemical cross-linking of the polymer network improves dimensional and mechanical stability, though it tends to restrict segmental motion and limit ionic conductivity (Özenler et al., 2025).

Among these approaches, modifying the polymer architecture through side-chain ether groups or comb-like and hyperbranched structures has proven particularly effective (Misenan et al., 2022; Nishimoto et al., 1998, 1999). This approach contributes to reducing the crystallinity of the material and promoting ionic transport within the polymer matrix while largely preserving the mechanical properties of the film.

Despite the advances reported in this field, the influence of comb-like branched architectures on the ionic conductivity of WPUs remains largely unexplored. In particular, studies addressing the combined effect of branched poly(ethylene oxide) segments and different LiCl concentrations in WPU-based electrolytes have not yet been reported. Since the incorporation of side-chain ether groups has been shown to reduce crystallinity and enhance ion transport in related polymer systems without significantly compromising material stability (Nishimoto et al., 1998, 1999), these structural modifications may represent a promising strategy for improving the electrochemical performance of WPU-based electrolytes. In this context, the present work focuses on the development of polymer electrolytes based on WPUs incorporating branched poly(ethylene oxide), with the aim of elucidating the effect of the branched architecture on ionic transport and optimizing the electrochemical properties of the system through the adjustment of lithium salt content. By addressing this knowledge gap, this study seeks to provide new insights into the design of WPU-based solid polymer electrolytes for lithium-ion battery applications.

2. Materials and methods

2.1. Chemical Materials

For the synthesis of the WPU, the reagents listed below were used: Poly(oxyethylene) (PEO 1500, molecular weight 1500, Sigma aldrich, USA), poly(ethylene glycol monomethyl ether)-based trimethylolpropane (Ymer N120, molecular weight 1000, Perstorp Co., Malmö, Sweden), 1,4-butanediol (1,4-BDO, Sigma aldrich, USA) was dehydrated in vacuum oven at 75 °C for 24 h. Isophorone diisocyanate (IPDI, Sigma Aldrich, USA), dibutyltin dilaurate (DBTDL, Sigma Aldrich, USA), ethilenediamine (EDA, Cicarelli, Argentina), 2 butanone (MEK, Cicarelli, Argentina) and lithium chloride (LiCl, Anedra, Argentina) were used as received.

All synthesis procedures were carried out in accordance with established laboratory safety protocols. Particular attention was paid to the handling of isocyanate-containing reagents and organic solvents, which were manipulated under adequate ventilation using appropriate personal protective equipment (PPE), including gloves, safety glasses, and laboratory coats. Waste solvents and residual chemical products generated during synthesis were collected and disposed of following institutional regulations and local environmental and safety guidelines.

Revista Tecnología y Ciencia
DOI: https://doi.org/10.33414/rtyc.57.49-70.2026 - ISSN 1666-6933

2.2. Synthesis of waterborne polyurethane

The WPU was synthesized using the prepolymer method, in which the diisocyanate is first reacted with polyols to form an isocyanate terminated prepolymer, followed by chain extension with a low molecular weight diol or diamine. The synthesis procedure is schematically illustrated in Figure 1. The formulation was based on IPDI (0.1908 mol), PEO (0.0445 mol), Ymer N120 (0.0318 mol), 1,4 BDO (0.0572 mol), and EDA (0.0572 mol).

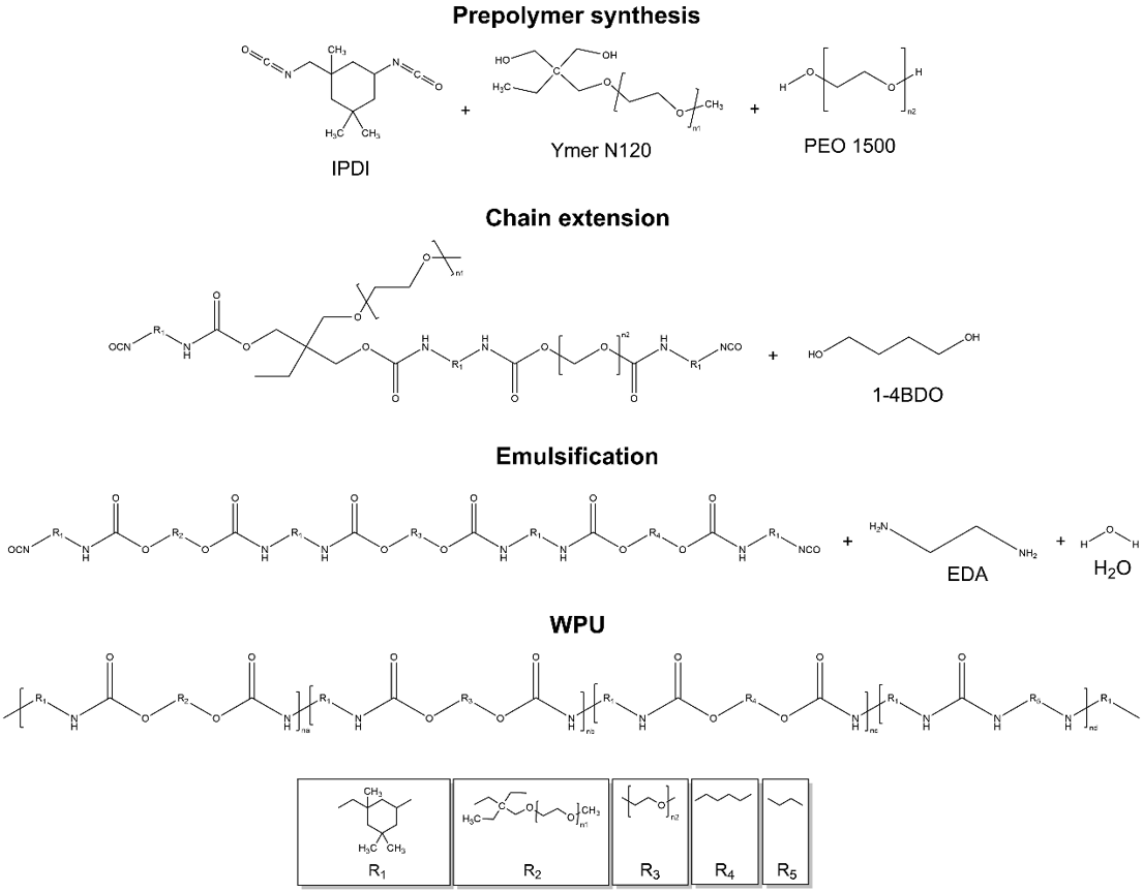


Figure 1. Schematic representation of WPU synthesis.

The prepolymer synthesis was conducted using a solution polymerization method, employing MEK as the reaction medium. The reaction was performed in a 500 mL three-neck glass reactor equipped with mechanical stirring at 150 rpm, a dry nitrogen inert atmosphere, a thermocouple for temperature control, a reflux condenser to prevent solvent loss, and a dropping funnel for the controlled addition of the reagents.

In the initial stage, PEO 1500 and Ymer N120 were charged into the reactor. The mixture was heated to 90 °C under continuous stirring with a constant flow of dry nitrogen for 60 min. These conditions promoted deoxygenation of the reaction medium and the removal of residual moisture traces. In this way, an inert environment was ensured and the likelihood of undesired side reactions was reduced.

Subsequently, the system temperature was decreased to 70 °C for the addition of IPDI and the DBTDL catalyst (0.3 wt% relative to the total polymer mass), both previously dissolved

Revista Tecnología y Ciencia
DOI: https://doi.org/10.33414/rtyc.57.49-70.2026 - ISSN 1666-6933

in MEK. The reaction was maintained under these conditions for 240 min to allow for the controlled progress of the polymerization. These parameters ensured adequate control over the reaction kinetics and medium viscosity, promoting the formation of urethane linkages between the IPDI and the polyols (PEO 1500 and Ymer N120).

For the first chain extension stage of the prepolymer, 1,4-BDO dissolved in MEK was added as a chain extender. The mixture was maintained at 70 °C for 120 min to ensure complete conversion of the reagent. Upon completion of this stage, the isocyanate-terminated prepolymer was cooled to 40 °C to proceed with the subsequent reaction step.

The chain extension in the aqueous medium was conducted by preparing a solution of EDA in deionized water to obtain a polymer dispersion with a solids content of 15 wt%. The prepolymer was slowly and carefully added to this solution, which promoted adequate dispersion in the aqueous medium and facilitated the chain-extension reaction. The process was conducted under constant stirring at 2000 rpm, while the temperature was maintained at 40 °C for 60 min. The corresponding reaction scheme is presented in Figure 2.

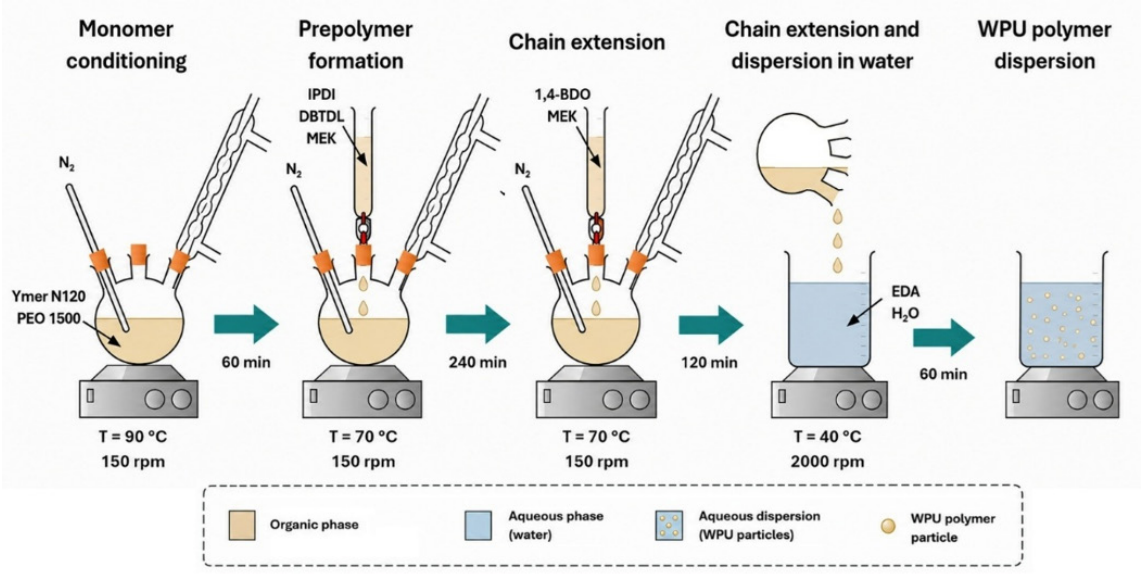


Figure 2. Experimental scheme for the synthesis of WPU.

2.3. Preparation of SPEs

The SPEs were obtained by incorporating different concentrations of LiCl into the previously synthesized WPU polymer dispersion under mechanical stirring to ensure adequate homogenization of the system.

LiCl was weighed inside an argon-filled glovebox (M. Braun Labstar). During the procedure, the levels of water and oxygen were maintained below 0.1 ppm. This protocol was adopted due to the highly hygroscopic nature of LiCl.

LiCl was dissolved in the WPU dispersion by continuous mechanical stirring for 1 h to ensure a homogeneous dispersion of the lithium salt within the polymeric medium. Four formulations were prepared by varying the LiCl content relative to the total polymer mass: SPE5 (5 wt%), SPE10 (10 wt%), SPE15 (15 wt%), and SPE20 (20 wt%).

The WPU dispersion and the SPE5, SPE10, SPE15, and SPE20 formulations were cast onto

Revista Tecnología y Ciencia
DOI: https://doi.org/10.33414/rtyc.57.49-70.2026 - ISSN 1666-6933

polytetrafluoroethylene (PTFE) molds and were dried at room temperature (25 °C) for 5 days. Subsequently, the resulting films were dried in a vacuum oven at 75 °C and 5 mmHg for 24 h to ensure the removal of residual moisture.

The dried polymer films of WPU, SPE5, SPE10, SPE15, and SPE20 were cut using a circular punch, obtaining discs with a diameter of 11 mm. The thickness of the films was measured using a Somet CSN25 1420 micrometer. Measurements were performed at different regions of each polymer film, and the obtained values were averaged to determine the representative thickness.

Subsequently, the WPU, SPE5, SPE10, SPE15, and SPE20 films were transferred to and stored in a glovebox under an argon atmosphere, maintaining moisture and oxygen concentrations below 0.1 ppm.

2.4. Characterization techniques

The polymerization reaction kinetics and SPEs compositions were analyzed by Fourier transform infrared (FT-IR) spectroscopy in the range of 4000-550 cm^{-1}. Spectra were acquired using a Shimadzu IRAffinity-1 spectrometer equipped with a QATR-10 single-reflection ATR accessory featuring a diamond crystal. Measurements were performed at room temperature with a resolution of 4 cm^{-1} and an average of 128 scans per spectrum.

The crystallinity of the polymer, the lithium salt, and the SPEs was characterized by X-ray diffraction (XRD) using a Panalytical X'Pert PRO diffractometer with Cu-Kα radiation (λ = 1.542 Å), operated at 45 kV and 45 mA.

Measurements were conducted in the 2θ range from 5° to 80° with a scan rate of 0.05° s^{-1}. The surface morphology of the WPU and SPE10 polymer films was analyzed by scanning electron microscopy (SEM, ESEM FEI Quanta 250) at an accelerating voltage of 20 kV. Samples were mounted onto aluminum stubs and sputter-coated with a thin gold layer to prevent charging effects during imaging. Each film had a thickness of approximately 350 µm and was prepared as 11 mm diameter circular discs. SEM images were acquired at 1000× magnification with a working distance of 9.8 mm.

Particle size distribution and zeta potential of the WPU dispersion were determined by dynamic light scattering (DLS) using a NICOMP Z3000 particle size analyzer (courtesy of Randon S.A.). Measurements were carried out at 23 °C using water as the dispersing medium (viscosity 0.923 cP, refractive index 1.333) and a laser wavelength of 632.8 nm. For particle size determination, an external fiber angle and a 90° scattering angle were employed, and three measurement cycles of 3 min each were recorded; samples were previously diluted in distilled water at a 1:100 ratio.

Electrophoretic mobility and zeta potential were determined using the same equipment under identical temperature, medium viscosity, and refractive index conditions, employing an external fiber angle of −19° and a scattering angle of −14.1368°. The dielectric constant of the medium, the electrode spacing, and the applied electric field strength were 78.5, 0.4 cm, and 4 V/cm, respectively.

Thermogravimetric analysis (TGA) and differential scanning calorimetry (DSC) were performed to evaluate the thermal stability and phase transitions of the materials. TGA was conducted using a TA Instruments Q500 analyzer from 30 to 600 °C at a heating rate of 20 °C min^{-1}, under a nitrogen atmosphere with a flow rate of 40 cm3 min^{-1}. DSC measurements were performed using a TA Instruments Q2000 calorimeter to determine the glass transition temperature (Tg) of the polymer. The DSC scans were recorded between -85 and 200 °C at a heating rate of 10 °C min^{-1} under a nitrogen flow of 50 cm^3 min^{-1}. Two heating/cooling cycles

Revista Tecnología y Ciencia
DOI: https://doi.org/10.33414/rtyc.57.49-70.2026 - ISSN 1666-6933

were performed, and the Tg values were determined from the second heating scan.

The ionic conductivity was determined by electrochemical impedance spectroscopy (EIS) using a Gamry Reference 3000 potentiostat/galvanostat. Measurements were performed in the frequency range from 0.01 Hz to 1 MHz, with an AC voltage amplitude of 10 mV at open-circuit voltage (OCV). All tests were conducted at room temperature (25 °C).

Three experiments were performed for each sample to assess data variability and ensure reproducibility. The WPU, SPE5, SPE10, SPE15, and SPE20 samples were analyzed. The films were placed between stainless steel blocking electrodes with a diameter of 11 mm, using a Swagelok-type cell assembled inside a glove box. The measuring cell consisted of a two-electrode, symmetrical stainless steel/polymer film/stainless steel configuration, housed in a PTFE body that ensured a fixed and reproducible contact area between the film and the electrodes, equal to the geometric area of the 11 mm diameter disc. Constant and uniform contact pressure between the electrodes and the film was maintained by means of the Swagelok fitting, and the entire cell was assembled and hermetically sealed under argon atmosphere prior to the EIS measurements.

All Nyquist plots obtained by EIS exhibited a semicircle in the high-frequency region and a straight line in the low-frequency region. The bulk resistance (Rb) of the electrolyte was determined from the Nyquist plot (real impedance vs. imaginary impedance) as the intersection point between the high-frequency semicircle and the low-frequency inclined line.

The ionic conductivity (σ, S cm^{-1}) of the samples was calculated using the following equation:

$$\sigma = \frac{L}{R_b . S} \tag{1}$$

Where R_b is the bulk resistance (Ω), L is the film thickness (cm), and S is the contact area of the film with the electrodes (cm^2).

3. Results and discussion

The WPU formulation employed in this study was selected based on previous investigations reported in the literature as well as preliminary experiments conducted by our research group, which demonstrated its ability to produce stable aqueous dispersions and mechanically robust films (Cui et al., 2024; Misenan et al., 2022). The present work specifically focuses on evaluating the influence of LiCl concentration on the electrochemical performance of this branched WPU system. Although variations in the content of branched poly(ethylene oxide) segments could also affect ionic transport properties, such optimization was considered beyond the scope of the present study and will be addressed in future work.

The polymerization reaction was monitored by FT-IR to determine the conversion of the monomers. The spectrum shows that increasing the reaction time produced a progressive decrease in the intensity of the band at 2255 cm^{-1} associated with the stretching of the isocyanate group (–NCO) (Figure 3). This change in the spectrum reflects the consumption of the isocyanate group and the formation of urethane linkages during the polymerization reaction (Cong et al., 2018).

Revista Tecnología y Ciencia
DOI: https://doi.org/10.33414/rtyc.57.49-70.2026 - ISSN 1666-6933

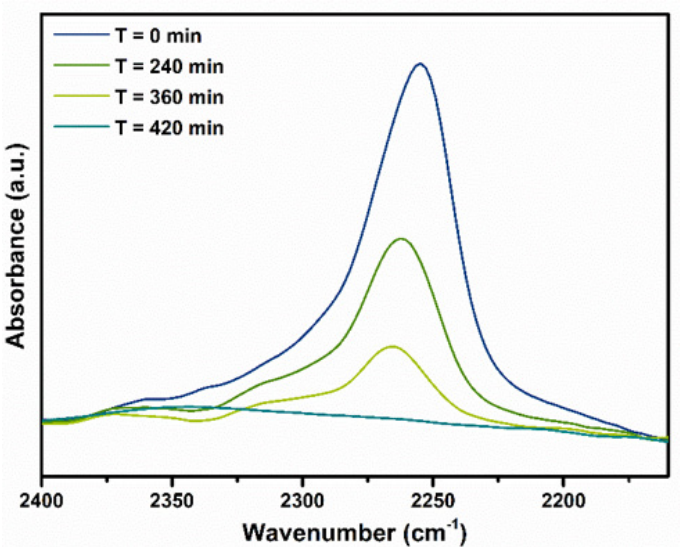


Figure 3. FT-IR spectra of WPU measured at different reaction times.

To assess the viability of these systems as SPEs, ionic conductivity was first evaluated as the key performance parameter. The WPU, SPE5, SPE10, SPE15, and SPE20 systems were characterized by EIS. Figure 4 presents the impedance spectra corresponding to the analyzed SPEs. All measurements were performed at room temperature (25 °C) and in triplicate to ensure the reproducibility of the results.

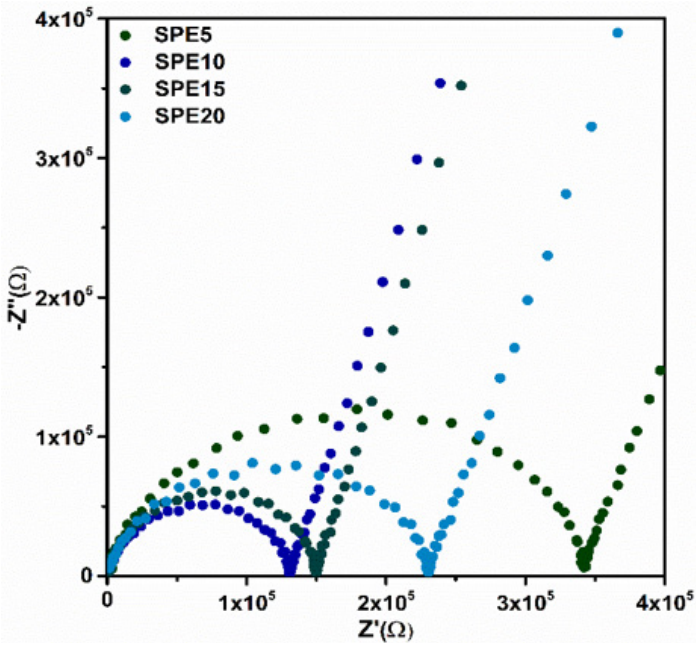


Figure 4 Complete Nyquist plot for SPE5, SPE10, SPE15 and SPE20.

The average (Rb) values obtained for the different SPEs are presented in Table 1. From these values, and following the methodology described previously, the average ionic conductivity of the SPEs was determined. The results are shown in Table 1 and Figure 5.

Revista Tecnología y Ciencia
DOI: https://doi.org/10.33414/rtyc.57.49-70.2026 - ISSN 1666-6933

Sample	R_b (Ω)	Ionic conductivity (S cm^{-1})
WPU	$1.03\ 10^{10}$	$3.81\ 10^{-12}$
SPE5	$3.43\ 10^{5}$	$1.08\ 10^{-7}$
SPE10	$1.31\ 10^{5}$	$2.82\ 10^{-7}$
SPE15	$1.50\ 10^{5}$	$2.46\ 10^{-7}$
SPE20	$2.30\ 10^{5}$	$1.61\ 10^{-7}$

Table 1. Rb and ionic conductivity of WPU, SPE5, SPE10, SPE15, and SPE20.

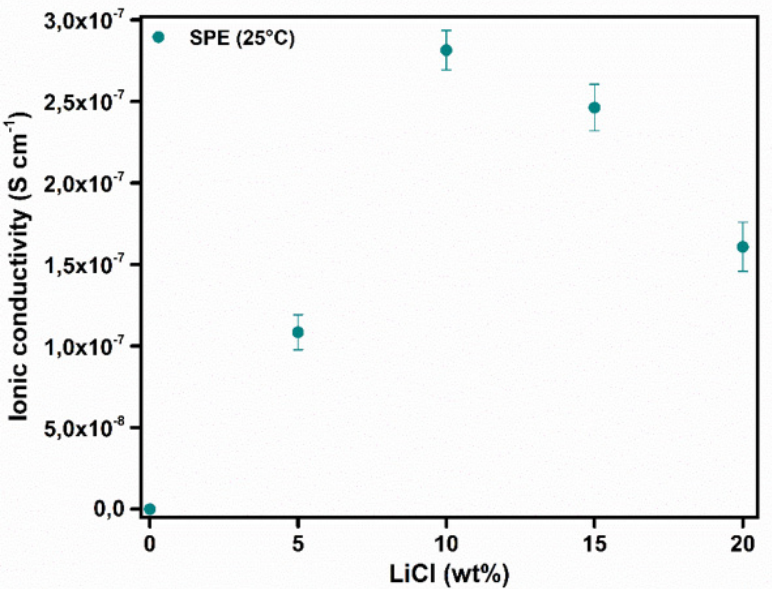


Figure 5. Ionic conductivity of the SPE systems with different LiCl contents.

The ionic conductivity of the system without lithium salt addition (WPU) was $3.81\ 10^{-12}$ S cm^{-1}. This material exhibits the characteristic behavior of an insulating material.

The SPEs showed an increase in ionic conductivity with increasing salt content, reaching a maximum value of $2.82\ 10^{-7}$ S cm^{-1} at a LiCl concentration of 10 wt%. Previous studies have demonstrated that at high salt concentrations (SPE15)) and (SPE20), a significant fraction of the ions may remain associated as ion pairs, reducing the number of free charge carriers and negatively affecting ionic conductivity (Bao, Shi, et al., 2018; Ng et al., 1998; Verma et al., 2014).

According to the literature, LiCl-based SPEs typically exhibit ionic conductivities in the range of 10^{-7} to 10^{-8} S cm^{-1} (Porcarelli et al., 2017; S. Wang et al., 2010; S. Wang & Min, 2010; Q. Zhang et al., 2021). In agreement with these studies, the SPE5, SPE10, SPE15, and SPE20 systems display ionic conductivity values within this range, highlighting their potential application as SPEs in LIBs.

Among the studied formulations, the system containing 10 wt% LiCl (SPE10) exhibited the highest ionic conductivity. Therefore, this composition was selected for further characterization using complementary techniques, as presented below, in order to elucidate the structural, thermal, and morphological features governing its behavior.

Revista Tecnología y Ciencia
DOI: https://doi.org/10.33414/rtyc.57.49-70.2026 - ISSN 1666-6933

The band quantification was performed by applying the Beer–Lambert law, whose validity for analyzing the absorption of the isocyanate group is well documented in the literature (Boufi et al., 1993; Elwell et al., 1996; Hua Fan et al., 1996). Comparisons between samples were conducted by normalizing the absorbance intensity of the band corresponding to the –NCO group with respect to an internal standard band, assigned to the $-CH_2$ stretching vibration at 2866 cm^{-1}, which remains invariant throughout the polymerization reaction (Cateto et al., 2008).

The conversion reached 40.21% after 240 min of reaction, corresponding to the prepolymer synthesis stage. Subsequently, following the incorporation of 1,4-BDO during the first chain extension stage, the conversion increased to 70.60% at 360 min. Finally, the addition of EDA during the chain extension stage in an aqueous medium allowed for the complete consumption of isocyanate groups, achieving 100% conversion at 420 min. These results confirm the total conversion of the reactants and the successful formation of the WPU system.

The colloidal stability of the synthesized WPU dispersion was evaluated by DLS. A mean particle size of 552 nm was obtained from a Gaussian fitted distribution (Figure 6). Particle size is an important parameter for evaluating the characteristics and stability of waterborne polyurethane dispersions and is strongly dependent on the chemical structure and hydrophilic content of the polyurethane system (Shi et al., 2022). The zeta potential of the dispersion was determined to be −11.43 mV. This relatively low value suggests that electrostatic repulsion is not the predominant stabilization mechanism in this system. This behavior is consistent with the absence of ionic internal emulsifiers such as carboxylate or sulfonate groups in the WPU formulation. In contrast, nonionic WPU dispersions can be stabilized through hydrophilic poly(ethylene oxide) segments that extend toward the aqueous phase and provide steric stabilization by hindering close approach and aggregation of the polymer particles (Santamaria-Echart et al., 2021). In the present system, the colloidal stability is therefore mainly attributed to the hydrophilic poly(ethylene oxide) chains derived from PEO 1500 and Ymer N120. These chains are expected to be preferentially located at the particle interface where their interaction with water can generate a hydrated steric layer around the particles. Similar behavior has been reported for PEO containing WPU systems in which hydrophilic EO segments are associated with the particle surface and influence the measured zeta potential (S.-Y. Chen et al., 2023). This nonionic stabilization mechanism is consistent with the stable aqueous dispersion and the homogeneous films obtained in this work.

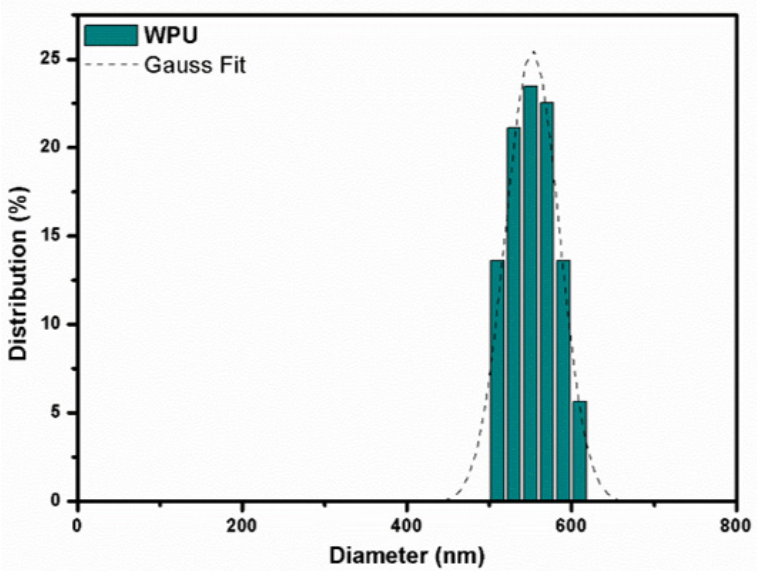


Figure 6. Particle size distribution of the WPU obtained by dynamic light scattering (DLS). The dashed line represents the Gaussian fit centered at a mean hydrodynamic diameter of 552 nm.

Revista Tecnología y Ciencia
DOI: https://doi.org/10.33414/rtyc.57.49-70.2026 - ISSN 1666-6933

The polymer film was characterized by FT-IR spectroscopy to elucidate its chemical structure (Figure 7). The spectrum displayed several characteristic absorption bands: including a band at 3337 cm^{-1} assigned to N–H stretching vibrations of secondary urethane groups; distinct bands in the 2950–2866 cm^{-1} region corresponding to the asymmetric and symmetric C–H stretching modes of CH_3 and CH_2 groups; a strong absorption at 1716 cm^{-1} attributed to urethane carbonyl stretching (amide I); and a band at 1667 cm^{-1} characteristic of urea carbonyl groups.

The amide II band was observed at 1536 cm^{-1}, associated with coupled C–N stretching and N–H bending vibrations. Additional features were identified at 1460 cm^{-1} (CH_2 scissoring), 1348 cm^{-1} (symmetric CH bending), 1302 cm^{-1} (combined N–H bending and C–N stretching), 1239 cm^{-1} (coupled N–H bending and C–H stretching), and in the 1096–944 cm^{-1} region (C–O–C stretching vibrations). These spectral assignments are in good agreement with previously reported literature data (Du et al., 2024; Mendes-Felipe et al., 2021; Peruzzo et al., 2011).

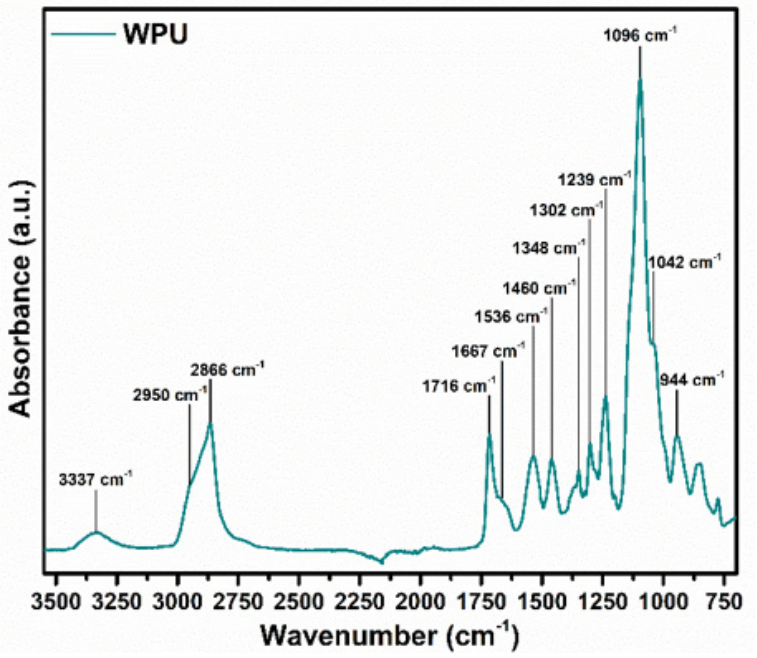


Figure 7. FT-IR spectra of WPU film.

As shown in Figure 8, the FT-IR spectra were normalized using the CH_2 stretching band at 2866 cm^{-1}, assuming that these groups are not affected by the presence of Li^+ ions (Cateto et al., 2008). The analysis revealed several modifications in the spectral bands. A decrease in intensity accompanied by a shift to lower wavenumbers was observed for the carbonyl (C=O) stretching band, from 1716 cm^{-1} (WPU) to 1697 cm^{-1} (SPE10), indicating coordination of Li^+ ions with carbonyl oxygen atoms and a reduction in free C=O groups (Bao, Qu, et al., 2018; Chen et al., 2022; Q. Zhang et al., 2021). Similarly, ether (C–O–C) bands showed reduced intensity and shifts to lower wavenumbers. The band at 1096 cm^{-1} (WPUB) shifted to 1091 cm^{-1} (SPE10), while the band at 1042 cm^{-1} (WPUB) shifted to 1038 for 10 wt% LiCl, suggesting Li^+ interaction with ether oxygen and a decrease in electron density (Cong et al., 2018; Mendes-Felipe et al., 2021; Santhosh et al., 2006). Overall, these changes support

Revista Tecnología y Ciencia
DOI: https://doi.org/10.33414/rtyc.57.49-70.2026 - ISSN 1666-6933

a coordination mechanism in which both C=O and C–O–C groups function as electron donors to Li^+ ions (Du et al., 2024; Misenan et al., 2022; Mustapa et al., 2021; Q. Zhang et al., 2021).

The analysis also revealed significant modifications in the amide II region. In the WPUB spectrum, the band at 1536 cm^{-1} showed a decrease in intensity and a shift toward higher wavenumbers, appearing at 1556 cm^{-1} for SPE10. Additionally, shifts were observed in other characteristic bands. The band at 1302 cm^{-1} in WPUB shifted to 1303 cm^{-1} in SPE10. Likewise, the band at 1239 cm^{-1} in WPUB was displaced to 1246 cm^{-1} for SPE10. These bands are associated with vibrational modes corresponding to C–N stretching and N–H bending (Bao et al., 2017; Chen et al., 2022; Mustapa et al., 2021; Santhosh et al., 2006). These variations are consistent with Li^+ coordination to the lone pairs on nitrogen atoms in urethane and urea groups. Such interactions diminish electron density around the nitrogen, subsequently weakening adjacent N–H bonds and modifying the C–N stretching force constants (Bao, Qu, et al., 2018; Du et al., 2024; Misenan et al., 2022; Mustapa et al., 2021).

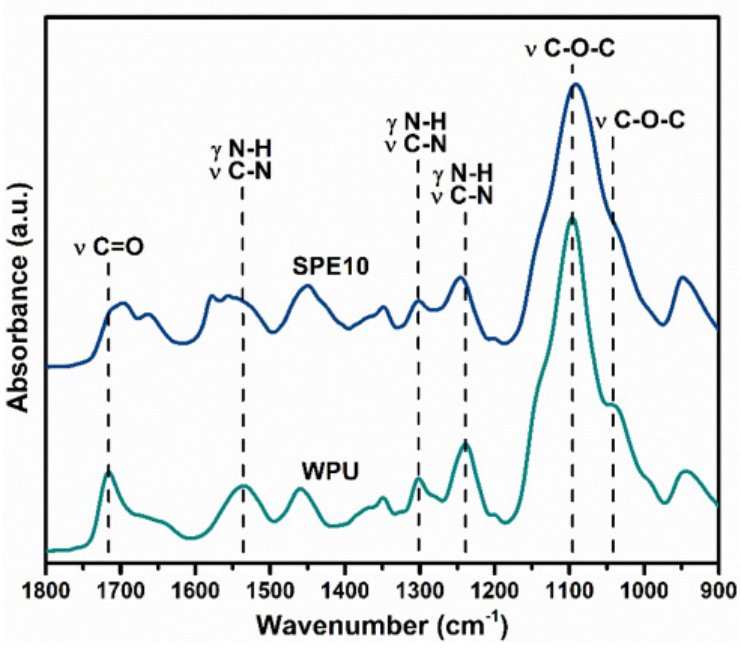


Figure 8. FT-IR spectra for WPU and SPE10 materials.

The crystallinity of the polymer, the lithium salt, and the SPEs was evaluated by XRD. WPU, SPE10, and LiCl samples were analyzed. As shown in Figure 9, the pure WPU polymer exhibits a broad and diffuse peak centered at $2\theta = 20.14°$, which is indicative of an amorphous structure. This behavior is typical of polyurethanes and is associated with the presence of ordered intra- and intermolecular hydrogen bonding within the polymer matrix (Bao, Qu, et al., 2018; Cui et al., 2022; Seo et al., 2020).

Revista Tecnología y Ciencia
DOI: https://doi.org/10.33414/rtyc.57.49-70.2026 - ISSN 1666-6933

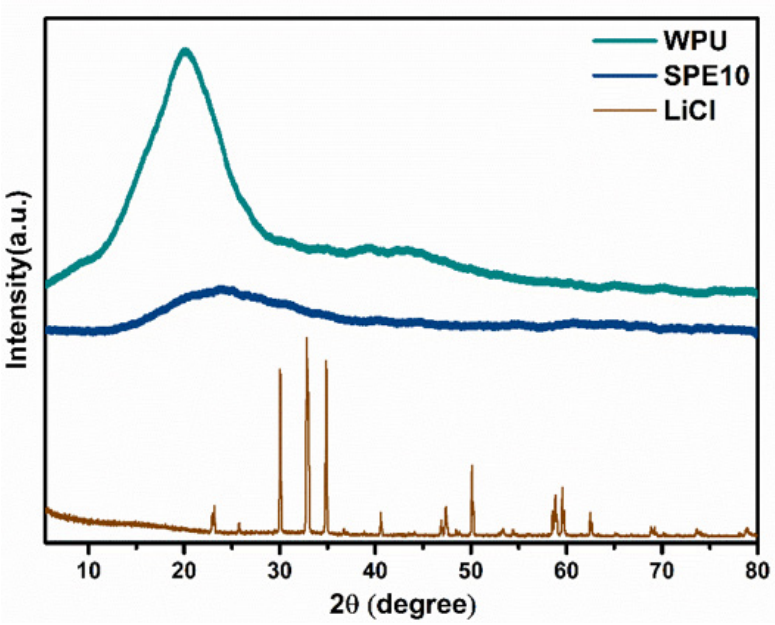


Figure 9. XRD patterns of WPU, SPE10, and LiCl samples.

The SPE10 sample exhibited a significant reduction in diffraction intensity compared to the WPU system, suggesting an increase in the amorphous character of the material upon salt addition. This behavior is attributed to the incorporation of lithium salt, whose presence disrupts polymer chain packing, reduces structural order, and promotes a higher amorphous fraction.

The amorphous phase in SPEs exhibits higher ionic conductivity than crystalline domains (Cui et al., 2024; Du et al., 2024; W. Zhang et al., 2021). This improvement is associated with the greater molecular flexibility of the amorphous structure, which enhances bond rotations and segmental motions (Fei et al., 2019; Hu et al., 2024; Mendes-Felipe et al., 2021; Seo et al., 2020). These effects facilitate ionic migration through the polymer matrix, thereby improving ionic transport properties (Cui et al., 2024; Du et al., 2024; Lv et al., 2022; D. Zhang et al., 2021).

Additionally, no characteristic diffraction peaks of LiCl were observed in the SPE10 pattern, suggesting that the salt is coordinated within the WPU polymer matrix (Bao, Qu, et al., 2018; Cui et al., 2024; Q. Zhang et al., 2021). The diffraction pattern of LiCl was also analyzed and compared with reference spectra from both the instrument library and the HighScore database, confirming that the obtained pattern corresponds to LiCl and that no secondary phases or impurities were detected. The main diffraction peaks were observed at (111) 30.05°, (200) 34.88°, (220) 50.16°, (311) 59.59°, (222) 62.48°, and (400) 73.63°, consistent with the characteristic crystallographic planes of the NaCl-type cubic structure (face-centered cubic, FCC).

The thermal properties of WPU and SPE10 were characterized by TGA and DSC. Differences in thermal stability, degradation stages, and the influence of LiCl on the glass transition temperature (Tg) of the polymer system were evaluated.

Figure 10 (a) presents the TGA curves of the WPU and SPE10 samples. For the WPU system, a T5% value of 294 °C was determined, whereas this value decreased significantly to 117 °C for SPE10.

Revista Tecnología y Ciencia
DOI: https://doi.org/10.33414/rtyc.57.49-70.2026 - ISSN 1666-6933

The initial degradation temperatures (Ti) also differed between samples, with values of 307 °C for WPU and 304 °C for SPE10. These changes in degradation temperatures are attributed to the presence of Li^+ ions, which accelerate thermal degradation processes through interactions with the polymer matrix (Bao et al., 2017; Cong et al., 2018; Mendes-Felipe et al., 2021).

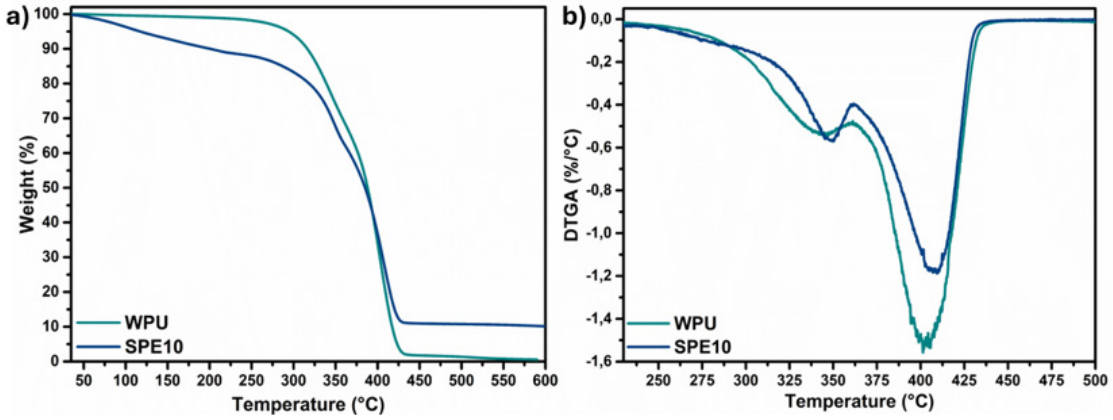


Figure 10. (a) Thermogravimetry curves of WPU and SPE10. (b) Derived from thermogravimetry curves.

Figure 10 (b) shows the DTGA curves. The WPU sample exhibits two main decomposition stages. The first stage, in the range of 245–261 °C, is attributed to the degradation of hard segments associated with urethane groups. The second stage, between 361 and 438 °C, corresponds to the degradation of soft segments of ether nature.

The SPE10 system also presents two decomposition stages. The first, in the range of 246–261 °C, is associated with the degradation of urethane segments, including both free groups and those interacting with Li^+ ions (Bao et al., 2017; Mendes-Felipe et al., 2021). The second stage, between 361 and 438 °C, is attributed to the degradation of ether-based soft segments, both free and coordinated with Li^+ ions (Bao et al., 2017; Bao, Qu, et al., 2018; Cong et al., 2018; Fei et al., 2019; Liu et al., 2020).

Although both systems exhibit similar degradation intervals, the incorporation of LiCl leads to changes in peak morphology. In particular, the maximum degradation temperature associated with urethane bonds shifted from 342 °C for WPU to 348 °C for SPE10. Similarly, the maximum corresponding to ether group degradation shifted from 403 °C in WPU to 407 °C in SPE10.

A system characterized by high thermal stability is a fundamental safety requirement for SPEs, as it prevents combustion and internal short circuits associated with polymer decomposition. Given that the typical operating temperature of LIBs remains below 80 °C, the materials employed in their fabrication must maintain stability within this temperature range (Bao, Qu, et al., 2018; Q. Zhang et al., 2021; Zheng et al., 2022). TGA analysis confirms that the SPE10 sample is thermally stable below 100 °C, thereby demonstrating its potential for LIB applications.

Figure 11 shows the glass transition temperatures corresponding to the soft segments (Tg,s), associated with ether groups, and to the hard segments (Tg,h), linked to urethane groups (Bao et al., 2017; Cong et al., 2018; Q. Zhang et al., 2021). The WPU and SPE10 samples exhibited Tg,s values of -48 °C and -41°C, and Tg,h values of 20 °C

Revista Tecnología y Ciencia
DOI: https://doi.org/10.33414/rtyc.57.49-70.2026 - ISSN 1666-6933

and 85 °C, respectively. Additionally, no endothermic peaks associated with crystalline melting transitions were observed, confirming the amorphous nature of the materials (Bao et al., 2017; P. Zhang et al., 2021).

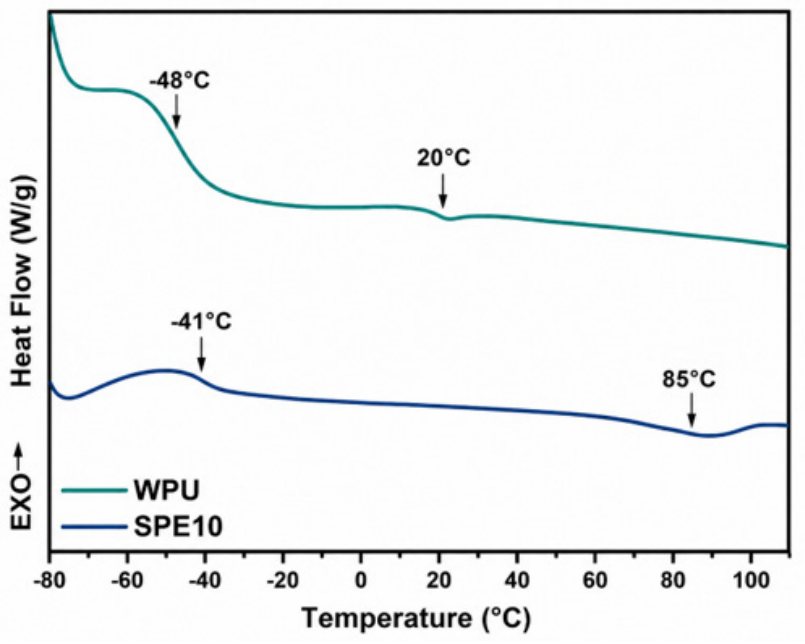


Figure 11 Differential scanning calorimetry of sample WPU and SPE10.

The observed increase in the Tg of both the soft and hard segments of the SPE10 sample, compared to the WPU system, is attributed to interactions between Li^+ ions and the oxygen atoms of the ether and urethane groups. These interactions produce an ionic coordination effect that shifts the glass transition temperatures toward higher values (Bao, Qu, et al., 2018; Chen et al., 2022; Cong et al., 2018; Q. Zhang et al., 2021).

For a polymer to function efficiently as a SPE, it must exhibit high ionic conductivity, which is achieved when Tg,s is below room temperature (Bandyopadhyay et al., 2010; Zheng et al., 2022). Since the Tg,s of SPE10 is lower than this temperature, the material satisfies this fundamental requirement, demonstrating its viability for SPE applications under ambient conditions.

Figure 12 (a) shows a photograph of the SPE10 film, which appears completely transparent, indicating a macroscopically homogeneous distribution of the lithium salt (LiCl) within the polymer matrix (Bao et al., 2017; Cong et al., 2018; Du et al., 2024).

Revista Tecnología y Ciencia
DOI: https://doi.org/10.33414/rtyc.57.49-70.2026 - ISSN 1666-6933

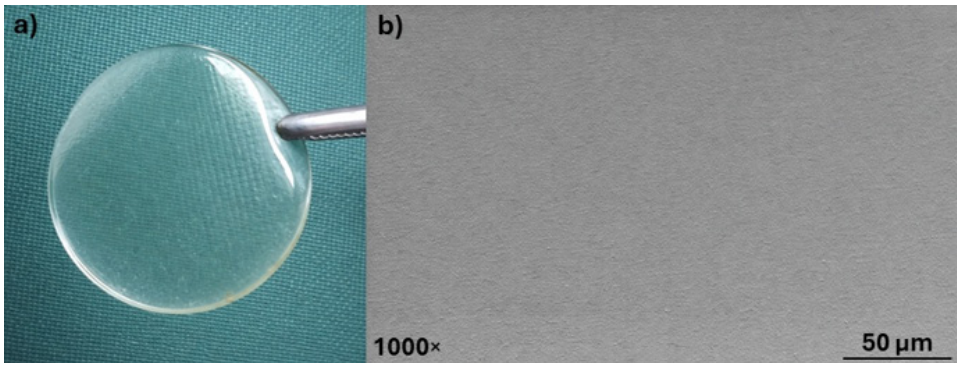


Figure 12 (a) Photograph of SPE10. (b) SEM image of the surface of SPE10.

Figure 12 (b) shows the SEM micrograph of the SPE10 system. The sample exhibits a smooth surface morphology lacking distinctive features, indicating a homogeneous structure and a uniform distribution of both the polymer matrix and the lithium salt. The absence of microphase separation confirms the miscibility of LiCl within the polymer system, evidencing its adequate compatibility (Cui et al., 2022; Du et al., 2024). Furthermore, these results are consistent with the FTIR-ATR, DSC, and XRD characterizations performed for the SPE10 sample.

While the SEM analysis discussed above characterizes the film surface, several complementary lines of evidence support a homogeneous distribution of LiCl throughout the bulk of the WPU matrix. The XRD pattern does not exhibit distinct crystalline reflections attributable to LiCl, suggesting that the salt is predominantly incorporated into the polymer matrix without the formation of detectable LiCl crystalline domains. In addition, the FTIR spectra show the characteristic changes associated with interactions between Li^+ and the polar groups of the polyurethane matrix, supporting the effective incorporation of the lithium salt into the polymer structure. The absence of distinct LiCl crystalline domains together with the observed thermal behavior and ionic conductivity further supports the homogeneous incorporation of LiCl within the WPU matrix. These findings are consistent with the smooth and featureless morphology observed in the surface SEM micrograph and collectively indicate good compatibility between LiCl and the WPU matrix.

4. Conclusion

WPU was successfully synthesized via the prepolymer method, achieving complete monomer conversion as confirmed by FT-IR spectroscopy. SPEs were prepared by incorporating LiCl into the WPU matrix. FT-IR analysis confirmed the formation of the polyurethane network and revealed favorable interactions between the polymer and LiCl. Specifically, Li^+ ions were found to coordinate with electron-donating nitrogen atoms (from C–N and N–H groups) and oxygen atoms (from C=O and C–O–C groups), indicating the successful formation of polymer–electrolyte complexes.

EIS analysis revealed an increase in ionic conductivity with increasing salt concentration. The maximum ionic conductivity was obtained for the SPE10 sample, with a value of $1.08\ 10^{-7}$ S cm^{-1}. For samples with 15 and 20 wt% LiCl, a decrease in ionic conductivity was observed.

Revista Tecnología y Ciencia
DOI: https://doi.org/10.33414/rtyc.57.49-70.2026 - ISSN 1666-6933

The obtained ionic conductivity values fall within the accepted range for LiCl-based SPEs, thereby demonstrating the material's potential application as an SPE in LIBs.

Complementary characterization techniques were employed to elucidate the effect of the lithium salt content (10 wt%) on the material structure and its influence on ionic conductivity. XRD and DSC characterization demonstrated that both WPU and SPE10 exhibit amorphous structures, which is advantageous for ion transport. The SPE10 film appeared macroscopically transparent and showed a homogeneous microstructure. Furthermore, SEM analysis revealed no evidence of phase separation, confirming good compatibility between the components. TGA analysis confirmed the thermal stability of SPE10, meeting the requirements for LIBs applications.

The results obtained in this study demonstrate the feasibility of employing branched WPU-based systems as SPEs for LIBs. Future research will focus on optimizing the polymer architecture by varying the content of branched poly(ethylene oxide) segments, as well as investigating the influence of other lithium salts and salt concentrations on ionic transport properties. Additionally, further studies will address the electrochemical stability window, lithium-ion transference number, and long-term cycling performance in complete battery cells. These investigations will contribute to a deeper understanding of the structure–property relationships governing ionic conductivity and will support the development of high-performance WPU-based solid polymer electrolytes for energy storage applications.

Revista Tecnología y Ciencia
DOI: https://doi.org/10.33414/rtyc.57.49-70.2026 - ISSN 1666-6933

Reference

Andersson, R., Hernández, G., See, J., Flaim, T. D., Brandell, D., & Mindemark, J. (2022). Designing polyurethane solid polymer electrolytes for high-temperature lithium metal batteries. *ACS Applied Energy Materials,* 5(1), 407–418. https://doi.org/10.1021/acsaem.1c02942

Bandyopadhyay, S., Marzke, R. F., Singh, R. K., & Newman, N. (2010). Electrical conductivities and Li ion concentration-dependent diffusivities, in polyurethane polymers doped with lithium trifluoromethanesulfonimide (LiTFSI) or lithium perchlorate (LiClO4). *Solid State Ionics,* 181(39–40), 1727–1731. https://doi.org/10.1016/j.ssi.2010.09.057

Bao, J., Qu, X., Qi, G., Huang, Q., Wu, S., Tao, C., Gao, M., & Chen, C. (2018). Solid electrolyte based on waterborne polyurethane and poly(ethylene oxide) blend polymer for all-solid-state lithium ion batteries. *Solid State Ionics,* 320, 55-63. https://doi.org/10.1016/j.ssi.2018.02.030

Bao, J., Shi, G., Tao, C., Wang, C., Zhu, C., Cheng, L., Qian, G., & Chen, C. (2018). Polycarbonate-based polyurethane as a polymer electrolyte matrix for all-solid-state lithium batteries. *Journal of Power Sources,* 389, 84–92. https://doi.org/10.1016/j.jpowsour.2018.04.020

Bao, J., Tao, C., Yu, R., Gao, M., Huang, Y., & Chen, C. (2017). Solid polymer electrolyte based on waterborne polyurethane for all-solid-state lithium ion batteries. *Journal of Applied Polymer Science,* 134(48). https://doi.org/10.1002/app.45554

Boufi, S., Belgacem, M. N., Quillerou, J., & Gandini, A. (1993). Urethanes and Polyurethanes Bearing Furan Moieties. 4. Synthesis, Kinetics, and Characterization of Linear Polymers. *Macromolecules*. 26(25), 6706-6717. https://doi.org/10.1021/ma00077a003

Cateto, C. A., Barreiro, M. F., & Rodrigues, A. E. (2008). Monitoring of lignin-based polyurethane synthesis by FTIR-ATR. *Industrial Crops and Products,* 27(2), 168–174. https://doi.org/10.1016/j.indcrop.2007.07.018

Chen, J., Liu, Z., Liu, J., Liu, X., Yang, X., & Jiang, X. (2022). A novel intrinsic flame-retardant and flexible polyurethane solid electrolyte for lithium batteries. *Materials Chemistry and Physics,* 279, 125763. https://doi.org/10.1016/j.matchemphys.2022.125763

Chen, S.-Y., Kokalari, I., Parnell, S. R., Smith, G. N., Zeng, B.-H., Way, T.-F., Chuang, F.-S., & Rwei, A. Y. (2023). Structure property relationship of micellar waterborne poly (urethane-urea): tunable mechanical properties and controlled release profiles with amphiphilic triblock copolymers. *Langmuir,* 39(29), 10033-10046. https://doi.org/10.1021/acs.langmuir.3c00921

Cong, B., Song, Y., Ren, N., Xie, G., Tao, C., Huang, Y., Xu, G., & Bao, J. (2018). Polyethylene glycol-based waterborne polyurethane as solid polymer electrolyte for all-solid-state lithium ion batteries. *Materials & Design,* 142, 221–228. https://doi.org/10.1016/j.matdes.2018.01.039

Cui, P., Li, Y., Liu, Y. X., Wang, S., Tang, X., Ye, Y., Su, H., & Sun, C. (2024). Polyether-based polyurethane electrolyte for lithium metal battery: a perspective. *RSC Advances*. 14(49), 36152–36160. Royal Society of Chemistry. https://doi.org/10.1039/d4ra06863g

Cui, P., Zhang, Q., Sun, C., Gu, J., Shu, M., Gao, C., Zhang, Q., & Wei, W. (2022). High ion conductivity based on a polyurethane composite solid electrolyte for all-solid-state lithium batteries. *RSC Advances*, 12(7), 3828–3837. https://doi.org/10.1039/d1ra07971a

Du, X., Guo, L., Tan, X., Wan, L., Tong, Y., Zhou, D., & Qin, Y. (2024). Self-healing polyurethane-based polymer electrolyte with high strength for all-solid-state lithium metal batteries. *Colloids and Surfaces A: Physicochemical and Engineering Aspects,* 680. https://doi.org/10.1016/j.colsurfa.2023.132703

Revista Tecnología y Ciencia
DOI: https://doi.org/10.33414/rtyc.57.49-70.2026 - ISSN 1666-6933

Elwell, M. J., Ryan, A. J., Grünbauer, H. J. M., & Lieshout, H. C. Van. (1996). An FT i.r. study of reaction kinetics and structure development in model flexible polyurethane foam systems. *Polymer*, 37(8), 1353-1361. https://doi.org/10.1016/0032-3861(96)81132-3

Fei, Y., Liu, S., Long, Y., Lu, L., He, Y., Ma, X., & Deng, Y. (2019). New single lithium ion conducting polymer electrolyte derived from delocalized tetrazolate bonding to polyurethane. *Electrochimica Acta*, 299, 902–913. https://doi.org/10.1016/j.electacta.2019.01.071

Fenton, D. E., Parker, J. M.; Wright, P. V. (1973). Complex of alkali metal ions with poly (ethylene oxide). *Polymer*, 14(11), 589. https://doi.org/10.1016/0032-3861(73)90146-8

Hu, J., Wang, W., Zhou, Y., Dong, B., He, S., Sun, J., Yan, H., Feng, Y., & Lu, L. (2024). Optimizing balance between ionic conductivity and mechanical performance in polyurethane type polymer electrolyte inducing stable interface for all-solid-state lithium battery. *Journal of Energy Storage*, 103. https://doi.org/10.1016/j.est.2024.114391

Hua Fan, L., Hu, C. P., Ping Zhang, Z., & Kang Ying, S. (1996). Polymerization Kinetics of Polyurethane and Vinyl Ester Resin Interpenetrating Polymer Networks by Using Fourier Transform Infrared Spectroscopy. *Journal of Applied Polymer Science*, 59(9), 1417-1426. https://doi.org/10.1002/(SICI)1097-4628(19960228)59:9<1417::AID-APP9>3.0.CO;2-E

Irfan, M., Atif, M., Yang, Z., & Zhang, W. (2021). Recent advances in high performance conducting solid polymer electrolytes for lithium-ion batteries. In *Journal of Power Sources* (Vol. 486). Elsevier B.V. https://doi.org/10.1016/j.jpowsour.2020.229378

Larrabide, A., Rey, I., & Lizundia, E. (2022). Environmental Impact Assessment of Solid Polymer Electrolytes for Solid-State Lithium Batteries. *Advanced Energy and Sustainability Research*, 3(10), 2200079. https://doi.org/10.1002/aesr.202200079

Li, J., Cai, Y., Wu, H., Yu, Z., Yan, X., Zhang, Q., Gao, T. Z., Liu, K., Jia, X., & Bao, Z. (2021). Polymers in Lithium-Ion and Lithium Metal Batteries. In *Advanced Energy Materials* (Vol. 11, Number 15). John Wiley and Sons Inc. https://doi.org/10.1002/aenm.202003239

Liu, X., Zhan, Y., Zhao, C., Su, Y., Ge, Z., & Luo, Y. (2020). A novel polymer electrolyte matrix incorporating ionic liquid into waterborne polyurethane for lithium-ion battery. *Polymers*, 12(7), 1513. https://doi.org/10.3390/polym12071513

Lv, Z., Tang, Y., Dong, S., Zhou, Q., & Cui, G. (2022). Polyurethane-based polymer electrolytes for lithium Batteries: Advances and perspectives. *Chemical Engineering Journal*, 430, 132659. https://doi.org/10.1016/j.cej.2021.132659

Mendes-Felipe, C., Barbosa, J. C., Gonçalves, R., Miranda, D., Costa, C. M., Vilas-Vilela, J. L., & Lanceros-Mendez, S. (2021). Lithium bis (trifluoromethanesulfonyl) imide blended in polyurethane acrylate photocurable solid polymer electrolytes for lithium-ion batteries. *Journal of Energy Chemistry*, 62, 485–496. https://doi.org/10.1016/j.jechem.2021.01.030

Misenan, M. S. M., Khiar, A. S. A., & Eren, T. (2022). Polyurethane-based polymer electrolyte for lithium ion batteries: a review. *Polymer International*, *71*(7), 751-769. https://doi.org/10.1002/pi.6395

Mustapa, S. R., Aung, M. M., & Rayung, M. (2021). Physico-chemical, thermal, and electrochemical analysis of solid polymer electrolyte from vegetable oil-based polyurethane. *Polymers*, 13(1), 1–20. https://doi.org/10.3390/polym13010132

Ng, S. T. C., Forsyth, M., MacFarlane, D. R., Garcia, M., Smith, M. E., & Strange, J. H. (1998). Composition effects in polyetherurethane-based solid polymer electrolytes. *Polymer*, 39(25), 6261–6268. https://doi.org/10.1016/S0032-3861(98)00153-0

Nishimoto, A., Agehara, K., Furuya, N., Watanabe, T., & Watanabe, M. (1999). High ionic conductivity of polyether-based network polymer electrolytes with hyperbranched side chains. *Macromolecules*, 32(5), 1541–1548. https://doi.org/10.1021/ma981436q

Revista Tecnología y Ciencia
DOI: https://doi.org/10.33414/rtyc.57.49-70.2026 - ISSN 1666-6933

Nishimoto, A., Watanabe, M., Ikeda, Y., & Kohjiya, S. (1998). High ionic conductivity of new polymer electrolytes based on high molecular weight polyether comb polymers. *Electrochimica Acta*, 43(10–11), 1177–1184. https://doi.org/10.1016/S0013-4686(97)10017-2

Özenler, S., Kiriy, N., Muza, U. L., Geisler, M., Kiriy, A., & Voit, B. (2025). Mechanically stable polymer networks incorporating polymeric ionic liquids for enhanced conductivity in solid-state electrolytes. *Designed Monomers and Polymers*, 28(1), 35–47. https://doi.org/10.1080/15685551.2024.2449444

Peruzzo, P. J., Anbinder, P. S., Pardini, O. R., Vega, J., Costa, C. A., Galembeck, F., & Amalvy, J. I. (2011). Waterborne polyurethane/acrylate: Comparison of hybrid and blend systems. *Progress in Organic Coatings*, 72(3), 429–437. https://doi.org/10.1016/j.porgcoat.2011.05.016

Porcarelli, L., Manojkumar, K., Sardon, H., Llorente, O., Shaplov, A. S., Vijayakrishna, K., Gerbaldi, C., & Mecerreyes, D. (2017). Single Ion Conducting Polymer Electrolytes Based On Versatile Polyurethanes. *Electrochimica Acta*, 241, 526–534. https://doi.org/10.1016/j.electacta.2017.04.132

Ram Prasanth S., Varatharajan Prasannavenkadesan, Vimal Katiyar, Ammathnadu Sudhakar Achalkumar; Polymer electrolytes: evolution, challenges, and future directions for lithium-ion batteries. RSC Appl. Polym. 2025; 3 (3): 499–531. https://doi.org/10.1039/d4lp00325j

Santamaria-Echart, A., Fernandes, I., Barreiro, F., Corcuera, M. A., & Eceiza, A. (2021). Advances in waterborne polyurethane and polyurethane-urea dispersions and their eco-friendly derivatives: A review. *Polymers*, 13(3), 409. https://doi.org/10.3390/polym13030409

Santhosh, P., Vasudevan, T., Gopalan, A., & Lee, K.-P. (2006). Preparation and properties of new cross-linked polyurethane acrylate electrolytes for lithium batteries. *Journal of Power Sources*, 160(1), 609–620. https://doi.org/10.1016/j.jpowsour.2006.01.091

Seo, Y., Jung, Y. C., Park, M. S., & Kim, D. W. (2020). Solid polymer electrolyte supported by porous polymer membrane for all-solid-state lithium batteries. *Journal of Membrane Science*, 603. https://doi.org/10.1016/j.memsci.2020.117995

Shi, Q., Wu, W., Yu, B., Ren, M., Wu, L., & Zhang, C. (2022). Preparation of ecofriendly water-borne polyurethane elastomer with mechanical robustness and self-healable ability based on multi-dynamic interactions. *RSC Advances*, 12(54), 35396–35408. https://doi.org/10.1039/d2ra07000f

Tang, S., Guo, W., & Fu, Y. (2021). Advances in composite polymer electrolytes for lithium batteries and beyond. *Advanced Energy Materials*, 11(2), 2000802. https://doi.org/10.1002/aenm.202000802

Tu, J., Wu, K., Jiang, J., Wu, M., Hu, Q., Xu, G., Lou, P., & Zhang, W. (2021). A novel ceramic/polyurethane composite solid polymer electrolyte for high lithium batteries. *Ionics*, 27(2), 569–575. https://doi.org/10.1007/s11581-020-03838-5

Verma, M. L., Minakshi, M., & Singh, N. K. (2014). Synthesis and characterization of solid polymer electrolyte based on activated carbon for solid state capacitor. *Electrochimica Acta*, 137, 497–503. https://doi.org/10.1016/j.electacta.2014.06.039

Wang, J., Li, S., Zhao, Q., Song, C., & Xue, Z. (2021). Structure Code for Advanced Polymer Electrolyte in Lithium-Ion Batteries. In *Advanced Functional Materials* (Vol. 31, Number 12). John Wiley and Sons Inc. https://doi.org/10.1002/adfm.202008208

Wang, S., Jeung, S., & Min, K. (2010). The effects of anion structure of lithium salts on the properties of in-situ polymerized thermoplastic polyurethane electrolytes. *Polymer*, 51(13), 2864–2871. https://doi.org/10.1016/j.polymer.2010.04.022

Wang, S., & Min, K. (2010). Solid polymer electrolytes of blends of polyurethane and polyether modified polysiloxane and their ionic conductivity. *Polymer*, 51(12), 2621–2628. https://doi.org/10.1016/j.polymer.2010.04.038

Revista Tecnología y Ciencia
DOI: https://doi.org/10.33414/rtyc.57.49-70.2026 - ISSN 1666-6933

Wu, J., Rao, Z., Cheng, Z., Yuan, L., Li, Z., & Huang, Y. (2019). Ultrathin, Flexible Polymer Electrolyte for Cost-Effective Fabrication of All-Solid-State Lithium Metal Batteries. *Advanced Energy Materials*, 9(46). https://doi.org/10.1002/aenm.201902767

Yang, Y., Li, W., Zhou, N., & Shen, J. (2020). Design and Construction of Cross-Linked PEO with the Integration of Helical Polyurethane as an Advanced All-Solid-State Polymer Electrolyte for Lithium Batteries. *Journal of Chemical Education*, 97(10), 3758–3765. https://doi.org/10.1021/acs.jchemed.0c00182

Yao, P., Yu, H., Ding, Z., Liu, Y., Lu, J., Lavorgna, M., Wu, J., & Liu, X. (2019). Review on polymer-based composite electrolytes for lithium batteries. *Frontiers in Chemistry*, 7, 522. https://doi.org/10.3389/fchem.2019.00522

Zhang, D., Li, L., Wu, X., Wang, J., Li, Q., Pan, K., & He, J. (2021). Research Progress and Application of PEO-Based Solid State Polymer Composite Electrolytes. In *Frontiers in Energy Research* (Vol. 9). Frontiers Media S.A. https://doi.org/10.3389/fenrg.2021.726738

Zhang, P., Guo, W., Guo, Z. H., Ma, Y., Gao, L., Cong, Z., Zhao, X. J., Qiao, L., Pu, X., & Wang, Z. L. (2021). Dynamically crosslinked dry ion-conducting elastomers for soft iontronics. *Advanced Materials*, 33(31), 2101396. https://doi.org/10.1002/adma.202101396

Zhang, Q., Wen, Y., Liu, K., Liu, N., Du, Y., Ma, C., Zhou, L., Liang, Y., & Jin, Y. (2021). Study of solid polyurethane electrolytes synthesized from HDI and PEO of different molecular weight. *Journal of Electroanalytical Chemistry*, 893. https://doi.org/10.1016/j.jelechem.2021.115305

Zhang, W., Wang, M., Zhao, H., Liu, X., Liu, R., Xie, X., & Wu, Y. (2021). Synthesis and characterization of electrolyte substrate materials based on hyperbranched polyurethane elastomers for anodic bonding. *Journal of Applied Polymer Science*, 138(35). https://doi.org/10.1002/app.50872

Zheng, T., Cui, X., Chu, Y., Li, H., & Pan, Q. (2022). Ultrahigh Elastic Polymer Electrolytes for Solid-State Lithium Batteries with Robust Interfaces. *ACS Applied Materials and Interfaces*, 14(4), 5932–5939. https://doi.org/10.1021/acsami.1c20243

Zhu, Y., Xiao, S., Shi, Y., Yang, Y., Hou, Y., & Wu, Y. (2014). A composite gel polymer electrolyte with high performance based on poly(vinylidene fluoride) and polyborate for lithium ion batteries. *Advanced Energy Materials*, 4(1). https://doi.org/10.1002/aenm.201300647

Contribución de los Autores

	Colaboración Académica													
Nombres y Apellidos del autor	1	2	3	4	5	6	7	8	9	10	11	12	13	14
Agustín Vergalito	x		x	x	x	x	x	x		x			x	x
Mariela Gisela Ortiz		x		x		x		x				x		
Francisco Martín Pardini		x		x		x		x				x		

1-Administración del proyecto, 2-Adquisición de fondos, 3-Análisis formal, 4-Conceptualización, 5-Curaduría de datos, 6-Escritura - revisión y edición, 7-Investigación, 8-Metodología, 9-Recursos, 10-Redacción - borrador original, 11-Software, 12-Supervisión, 13-Validación, 14-Visualización.

El presente trabajo de investigación se realizo en el marco del Doctorado de Ingeniería, mención Materiales, Facultad Regional La Plata, Universidad Tecnológica Nacional, Argentina.

This research was conducted as part of a PhD in Engineering with a specialization in Materials at the La Plata Regional Faculty of the National Technological University, Argentina.